Physics of Plasmas

Toroidal gyro-Landau fluid model turbulence simulations in a nonlinear ballooning mode representation with radial modes

R. E. Waltz, G. D. Kerbel and J. Milovich

View Online   Export Citation

ARTICLES YOU MAY BE INTERESTED IN

Physics of Plasmas   Physics of Fluids
Special Topic: Turbulence in Plasmas and Fluids
Submit Today!

AIP Publishing
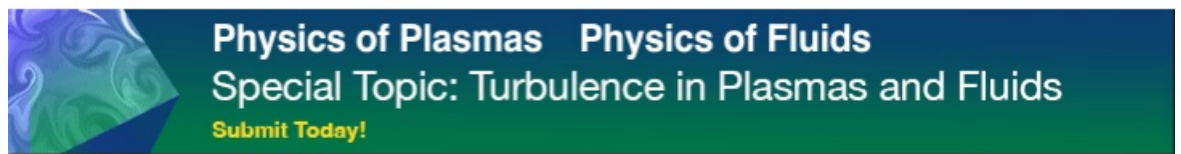
Toroidal gyro-Landau fluid model turbulence simulations in a nonlinear ballooning mode representation with radial modes

R. E. Waltz
General Atomics, P.O. Box 85608, San Diego, California 92186-9784

G. D. Kerbel and J. Milovich
NERSC at Lawrence Livermore National Laboratory, Livermore, California

The method of Hammett and Perkins [Phys. Rev. Lett. **64**, 3019 (1990)] to model Landau damping has been recently applied to the moments of the gyrokinetic equation with curvature drift by Waltz, Dominguez, and Hammett [Phys. Fluids B **4**, 3138 (1992)]. The higher moments are truncated in terms of the lower moments (density, parallel velocity, and parallel and perpendicular pressure) by modeling the deviation from a perturbed Maxwellian to fit the kinetic response function at all values of the kinetic parameters: $k_\| v_{th}/\omega$, $b = (k_\perp \rho)^2/2$, and ω_D/ω. Here the resulting gyro-Landau fluid equations are applied to the simulation of ion temperature gradient (ITG) mode turbulence in toroidal geometry using a novel three-dimensional (3-D) nonlinear ballooning mode representation. The representation is a Fourier transform of a field line following basis (k_y', k_x', z') with periodicity in toroidal and poloidal angles. Particular emphasis is given to the role of nonlinearly generated $n = 0$ $(k_y' = 0, k_x' \neq 0)$ "radial modes" in stabilizing the transport from the finite-n ITG ballooning modes. Detailing the parametric dependence of toroidal ITG turbulence is a key result.

I. INTRODUCTION

Turbulence among ion temperature gradient (ITG) modes is thought to be a useful paradigm for understanding some of the most important features of transport in tokamaks. While such modes are essentially fluid-like in nature, kinetic effects such as Landau resonances in the parallel and curvature drift motion as well as finite Larmor radius (FLR) have some important quantitative effects. Fluid models have found wide use in simulating plasma turbulence because of their simplicity and tractability. Such models advance a few moments of a kinetic equation rather than the full velocity distribution function. Until the work of Hammett and Perkins,[1] it was not widely appreciated that kinetic effects such as Landau damping could be represented by truncating the fluid hierarchy with the addition of a collisionless heat conductivity $[\chi = (2/\sqrt{\pi})v_{th}/|k_\||]$. Taking moments of the nonlinear electrostatic gyrokinetic equation this earlier $\mathbf{E} \times \mathbf{B}$ and parallel motion result has been generalized to include large gyromotion[2–4] and in particular Waltz, Dominguez, and Hammett[4] have added the curvature drift and resonance effects required for toroidal geometry. This yields nonlinear fluid equations for the gyrodensity, parallel motion, and pressures. The procedure for truncating the higher fluid moments involves a highly constrained fit to the linear kinetic response function at both large and small values of the kinetic parameters for parallel, gyro-, and curvature motion: $k_\| v_{th}/\omega$, $b = (k_\perp \rho)^2/2$, and ω_D/ω. Taking adiabatic electrons, such gyro-Landau fluid (GLF) models for the ions show excellent agreement with kinetic calculations of ITG local (constant $k_\|$ and ω_D) linear stability.[4]

This paper focuses on the application of GLF models for ITG turbulence in toroidal geometry using a novel three-dimensional (3-D) nonlinear ballooning mode representation. The most important parametric scaling features of ITG turbulence in a "slab" limit without curvature are probably well described by the simple fluid model simulations of Hamaguchi and Horton.[5] However, apart from some early and very limited work with simple fluid models by Horton et al.[6] and Waltz[7] there has not been enough work simulating ITG turbulence in toroidal geometry to understand its parametric dependence. As useful as preliminary slab studies have been, the lower threshold, larger linear growth rates and radial mode widths imply that ITG turbulent transport in actual toroidal geometry should be considerably larger and perhaps have different parametric dependencies. An exploratory mapping of these parametric dependencies is the final product of this paper. A key physical caveat to this and previous work is that it has become customary and convenient to limit discussion of ITG turbulence to pure ion plasmas with adiabatic electron motion, thus direct comparison with experiments should be limited.

Most of the previous work in toroidal geometry has been done using the conventional multiple helicity (m,n,r) representation[7,8] either in covering the whole plasma or an annulus. While this is a natural representation for slab or interchange-like modes with no linear interaction from the curvature coupling and even limited nonlinear interaction between singular surfaces at different m/n helicities, toroidally coupled ballooning modes span many singular surfaces. The conventional multiple helicity code is best suited for a global full radius plasma simulation. However, it is presently too difficult to span the full spectrum of drift modes at realistic values of the relative gyroradius. At realistic relative gyroradius, such codes are forced to operate over a narrow band of helicities or radial annulus. Only cyclic radial boundary conditions are natural to the description of radially homogeneous turbulence. An eddy leaving one side of the annulus is assumed to harmlessly appear on the other side provided the radial correlation length is smaller than the width of the annulus. This immediately leads to a Fourier transform repre-

sentation. The three-dimensional ballooning mode representation (BMR) used here involves a Fourier transform in the cross-field directions of the Cowley et al.[9] field line following "twisted eddy basis" and unlike the (m,n,r) basis it is the natural basis for linear normal modes in toroidal geometry, i.e., ballooning modes. Fourier representations provide a very convenient description of GLF model dissipation and gyroradius effects. (Both are in fact awkward to represent on a radial grid.) However, a key physical assumption in the use of a radial Fourier transform representation is that the turbulence is in fact homogeneous and no turbulent energy is allowed to propagate away from the annulus (although it may propagate through the annulus). This approximation is difficult to assess and should be a concern of future work.

The formulation and numerical implementation of the nonlinear ballooning mode representation has undergone intense recent development by the present authors[10] as well as Beer et al.[11] and Hammett et al.,[12] and we believe that it is now well understood. In particular an efficient numerical method[11] for enforcing poloidal periodicity is now well in hand. A related real space "flux tube" field line following basis has been used by Parker et al.[13] in a comparison of gyrokinetic and gyrofluid simulations in both slab and toroidal geometry.

Particular emphasis in this paper is given to the enormous importance of "radial" modes in determining the nonlinear saturation of the turbulence. Radial modes have $n=0$ toroidal mode number in contrast to the finite-n ballooning modes. They correspond to sheared poloidal and toroidal rotations within the flux surfaces but also have corresponding pressure perturbations which alternately steepen and flatten the local pressure gradient driving the ballooning modes. They are "near" equilibria with frequency and parallel wave number close to zero, but differ from the $n=0$ equilibrium because they have a finite radial wave number corresponding to wave lengths on the scale of the gyroradius rather than the radius of the plasma. They cause no transport directly but their sheared $\mathbf{E}\times\mathbf{B}$ rotations have a strong stabilizing effect on the finite-n ballooning modes causing the diffusion. The radial modes are nonlinearly driven by the ballooning modes. Diamond and Kim[14] have called this nonlinear Reynolds stress effect "eddy sheared flow generation" and it has been woven into an edge turbulence self-regulating shear flow model for low- to high-mode (L–H) transitions by Diamond et al.[15] The effects have been seen in simulations of resistive interchange mode turbulence at the edge by Carreras, Lynch, and Garcia[16] and by Guzdar et al.[17] Such nonlinearly generated sheared rotational flows were also seen in early studies of core turbulence by Hasagawa and Wakatani[18] and referred to as "self-organizing" flow.

There are several problems in the treatment of radial modes or nonlinearly generated shear flows. It is unclear in much previous work how to separate the scales of the "radial" modes from the equilibrium rotation which evolves on a transport time scale and is driven by momentum sources. Avoiding the slow evolution of the equilibrium was a key reason why $(m,n)=(0,0)$ modes were simply left out of most (m,n,r) simulations (Ref. 7 is but one example). The ballooning mode representation naturally involves a radial

Fourier transform so that scale separation is easily defined. A second key problem for radial modes in ITG core turbulence is the correct form for the adiabatic electron response. Dorland et al.[19] and also Beer et al.[11] have emphasized that electrons cannot respond adiabatically when the parallel wave number is zero. Thus the electron density perturbations should have an adiabatic or Boltzmann response only to potential perturbations deviating from the flux surface average potential. Finally, the saturated amplitudes of the radial modes are ultimately determined by the physical linear damping mechanism. In this paper we take the dominant damping process to be the Landau damping associated with the geodesic curvature drift motion and not magnetic pumping as previously suggested. In essence the radial modes are assumed to follow the same GLF model equations of motion assigned to the finite-n ballooning modes.

The importance of sheared equilibrium $\mathbf{E}\times\mathbf{B}$ (or more precisely Doppler shift) rotations in stabilizing turbulence at the tokamak edge[20] is now well appreciated experimentally.[21] It appears that the general condition for the shear rate to be comparable to the maximum linear growth rate (without Doppler shear) may even in some instances be satisfied in the core plasma where rotations are nearly toroidal. There is some experimental evidence in this direction from magnetic braking experiments on DIII-D.[21,22] The effect of $\mathbf{E}\times\mathbf{B}$ shear on slab ITG turbulence has been treated in many recent papers.[23–25] In this paper we show how the stabilizing effect of $\mathbf{E}\times\mathbf{B}$ can be treated in the context of toroidal geometry using the ballooning mode representation. The important destabilizing effect of parallel shear flow is consistently included for purely toroidal rotation.

As noted, our final product is to explore the parametric dependence of toroidal ITG turbulent transport on shear, safety factor, and toroidicity, as well as relative temperature gradients. We shall address a number of questions: Can the standard linear mixing length rules provide a useful summary of the simulations? The linear mixing length rules posit that the transport scales like the product of linear growth rate and radial width squared of the most unstable linear mode. Does the transport have a gyro-Bohm or Bohm-like scaling, i.e., does the mixing length scale to an intrinsic length like the gyroradius or to a extrinsic length like the plasma radius? Is there subcritical transport below the critical temperature gradient? Previous two-dimensional local toroidal ITG model simulations[26] found evidence of subcritical transport. How restrictive are the model assumptions of pure ion plasma and adiabatic electrons for a typical Tokamak Fusion Test Reactor (TFTR) L-mode discharge?

In outline Sec. II precisely defines the GLF model equations for toroidal geometry. Section III describes the nonlinear ballooning mode representation and how to deal with periodicity for both finite-n and radial modes. Section IV briefly describes the formulation of equilibrium scale sheared rotations in the context of ballooning modes. Section V provides the main body of the work with many numerical illustrations. Our conclusions are summarized in Sec. VI. We should note that Ref. 10 can be read as a preliminary version of this work. While some aspects of the formulation are repeated here for convenience, the results of the present paper

differ in some important details which we shall point out when appropriate.

II. GLF EQUATIONS FOR TOROIDAL GEOMETRY

A derivation of the GLF model equations for toroidal geometry is given in Ref. 4. For completeness we summarize it here to define the model. The model follows from taking moments of nonlinear gyrokinetic equations for perturbed density N_k, parallel motion U_k, and pressures $P_{\|k}$, $P_{\perp k}$ of the gyrocenters. The higher-order perturbed moments are closed as linear combinations of the lower moments by first assuming a perturbed Maxwellian and then adding "Maxwellian deviations" fitted to the kinetic response function. The resulting equations of ion motion are

$$\frac{dN_k}{dt} = -i\omega_*[(\hat{1}-\hat{\eta})\phi_{1k}+\hat{\eta}\phi_{2k}]+i\omega_D\phi_{12k}-i\hat{k}_\|U_k$$
$$+\frac{i\omega_D\tau^{-1}(P_{\|k}+P_{\perp k})}{2}, \tag{1}$$

$$\frac{dU_k}{dt} = -i\hat{k}_\|(\tau^{-1}P_{\|k}+\phi_{1k})+i\omega_D\tau^{-1}$$
$$\times\left[\left(\frac{1}{2}\right)(\Gamma_\|+\Gamma_\perp)U_k-i\sigma_t uT_{\|k}\right], \tag{2}$$

$$\frac{dP_{\|k}}{dt} = -i\omega_*(\hat{1}\phi_{1k}+2\hat{\eta}\phi_{2k})+iX_\|\omega_D\phi_{12k}-i\hat{k}_\|[\Gamma_\|U_k$$
$$-i\sigma_s\chi_1^\|T_{\|k}]+i\omega_D\tau^{-1}\left[X_\|P_{\|k}+\left(\frac{3}{2}\right)T_{\|k}\right.$$
$$\left.+\left(\frac{1}{2}\right)T_{\perp k}-i\sigma_t(\nu_\|^\|T_{\|k}+\nu_\perp^\|T_{\perp k})\right], \tag{3}$$

$$\frac{dP_{\perp k}}{dt} = -i\omega_*[(\hat{1}-\hat{\eta})\phi_{2k}+2\hat{\eta}\phi_{3k}]+iX_\perp\omega_D\phi_{23k}$$
$$-i\hat{k}_\|[\Gamma_\perp U_k-i\sigma_s\chi_1^\perp T_{\perp k}]+i\omega_D\tau^{-1}\left[X_\perp P_{\perp k}\right.$$
$$\left.+T_{\perp k}+\left(\frac{1}{2}\right)T_{\|k}-i\sigma_t(\nu_\|^\perp T_{\|k}+\nu_\perp^\perp T_{\perp k})\right], \tag{4}$$

where the terms with brackets [ ] represent higher moments containing the Maxwellian deviations. The latter have coefficients $\chi_1^\|=2\chi_1^\perp=2\sqrt{2}/\sqrt{\pi}$ for parallel motion, and $\mu=(0.80-0.57i\sigma_t)$, $\nu_\|^\|=\nu_\perp^\|=(1-i\sigma_t)$, $\nu_\perp^\|=\nu_\perp^\perp=0$ for curvature motion (with $\sigma_s=k_\|/|k_\||$, $\sigma_t=\omega_D/|\omega_D|$). The gyroaveraged electric potentials are given in terms of modified Bessel functions

$$\phi_{1k}=\Gamma_0\phi_k, \tag{5}$$

$$\phi_{2k}=[\Gamma_0-b(\Gamma_0-\Gamma_1)\phi_k], \tag{6}$$

$$\phi_{3k}=\tfrac{1}{2}[(2-4b+b^2)\Gamma_0-(5b-2b^2)\Gamma_1+b^2\Gamma_2]\phi_k, \tag{7}$$

with $\phi_{12k}=(\phi_{1k}+\phi_{2k})/2$ and $\phi_{23k}=(\phi_{2k}+\phi_{3k})/2$ and $\phi_k=(e/T_e)\Phi_k$. The gyrodensity is given by the quasineutrality relation

$$N_k=n_k/n_0+\tau(\phi_k-\phi_{1k}), \tag{8}$$

where n_k is the physical ion density perturbation and the second term is the polarization drift. The perturbed temperature is $T_k=P_k-N_k$ and $\tau^{-1}=T_i/T_e$.

To model ITG or η_i-mode turbulence, we take the adiabatic response to be

$$n_k/n_0=(\phi_k-\langle\phi_k\rangle), \tag{9}$$

where $\langle\phi\rangle$ is the flux surface average normed potential perturbation. For finite-n ballooning modes $\langle\phi\rangle=0$ but for $n=0$ radial modes it is important to realize that density can only have a Boltzmann-like response to deviations from the average potential along a field line.[19,11] If $k_\|$ is identically zero then there is no response ($n_k/n_0=0$). In Ref. 10 the density perturbations for radial modes were assumed to have no response. This leads to large nonlinear pumping of the radial modes. In contrast a unit response ($n_k/n_0=\phi_k$) leads to rather small nonlinear pumping and small amplitude radial modes. A better model is given by Eq. (9) (which is in between no response and unit response) but it must be kept in mind that a simple adiabatic electron response for ITG turbulence is merely an academic convenience to be repaired in subsequent work. The danger of this approximation is illustrated further in Sec. V C.

The adiabatic compression indices are $\Gamma_\|=3$, $\Gamma_\perp=1$, $X_\|=2$, $X_\perp=3/2$. It is particularly important to retain the detailed compression model since at low k_y, the ITG threshold is sensitive to these indices. For one-dimensional parallel motion only (i.e., slab geometry) $\Gamma_\|=3$ suggests $\eta_{i\_crit}=\Gamma_\|-1=2$ whereas for three-dimensional curvature drift motion important for toroidal geometry, we have $\Gamma=\Gamma_\|+(2/3)\Gamma_\perp=5/3$ [and $(1/3)X_\|+(2/3)X_\perp=5/3$] so $\eta_{i\_crit}=\Gamma-1=2/3$ which is much lower. Keeping all these different compression indices requires a two-pressure model.

The equations of motion require further definition. Here and throughout we use a system of units with $c_s=(T_e/M)^{1/2}$ the unit of velocity, $\rho_s=c_s/\Omega$ the unit of microlength, a (the minor radius) the unit of macrolength, and a/c_s the unit of time. The cross-field wave numbers in and across the flux surface $k=(k_y,k_x)$ are normed to ρ_s^{-1}. The parallel wave number $k_\|$ is normed to a^{-1} and the major radius R to a. The density gradient is given by $1=a/L_n$, the temperature gradient by $\hat{\eta}=a/L_T$ ($\eta_i=\hat{\eta}/1$) The normalized electron diamagnetic frequency is $1k_y$ with $\omega_*=k_y$. The normed curvature drift frequency $\omega_D=\omega_*\mathbf{g}$ where $\mathbf{g}=(2/R)$ $[\cos\theta+(k_x/k_y)\sin\theta]$ represents the local normal and geodesic curvature at the poloidal angle θ.

We use a "simple gyroaverage model" valid linearly to all orders in b in shearless geometry. In a sheared magnetic field the parallel wave number has a first order in b gyrocorrection given by

$$\hat{k}_\|=k_\|-ik_s[(k_y/k_x)/k_\perp^2]b\Gamma_0'(b)/\Gamma_0(b) \tag{10}$$

(where $k_s=\hat{s}/Rq$ and $\hat{s}=d\ln q/d\ln r$). This approximates the Linsker effect[27] which averages out the shear with a gyroradius of a singular surface. Simple nonlinear $\mathbf{E}\times\mathbf{B}$ convective time derivatives are given by

$$\frac{df_k}{dt} = \frac{\partial f_k}{\partial t} - \sum_{k1} (k_{x1}k_{y2} - k_{x2}k_{y1})\phi_{k1}f_{k2}, \tag{11}$$

with $\mathbf{k}_2 = \mathbf{k} - \mathbf{k}_1$ and all perturbed fields are normed to ρ_s/a. This approximate nonlinear coupling is valid at low $k_\perp$ but probably overestimates the coupling with gyroeffects by 20% to 30% at $k_\perp = 2$ (see Ref. 4). Including the truncation effect would weaken the nonlinear coupling and likely increase the turbulence levels and transport.

A more accurate "full gyroaverage" model valid through first order in b is described by Dorland et al.[3] It handles the Linsker effect implicitly and contains additional nonlinear FLR effects including a nonlinear hyperviscosity ($k_\perp^4$ damping) due to the Landau resonance in the gyromotion. A six-moment "full gyroaverage" model (rather than four) for toroidal geometry has been developed by Hammett et al.[12] and gives extremely accurate linear normal mode comparisons to kinetic theory. The four-moment simple gyroaverage model used here appears to typically underestimate linear growth rates and radial mode widths compared to kinetic theory so that mixing length diffusion estimates could be as much as a factor 2× smaller. (This is detailed in Sec. VA.) Thus from both linear and nonlinear considerations we expect the transport from the simple model to underestimate the full GLF model and kinetic particle simulations. The advantage of the simpler models is that while less accurate, they are 2–3× faster to simulate and it would be very surprising if their parametric dependence is different.

In physical units, the plasma flux is given by

$$\Gamma_{px} = n_0 \sum_k \left(\frac{n_k}{n_0}\right)^* \left(\frac{-ik_y c\Phi_k}{B}\right), \tag{12}$$

and the energy flux

$$\Gamma_{Ek} = \left(\frac{3}{2}\right)p_0 \sum_k \left(\frac{p_k^a}{p_0}\right)^* \left(\frac{-ik_y c\Phi_k}{B}\right), \tag{13}$$

where $p_k^a/p_0 = [(1/3)p_{\|k}/p_0] + [(2/3)p_{\perp k}/p_0]$, with the physical pressures given by $p_{\|k}/p_0 = P_{\|k} - \tau(\phi_k - \phi_{1k})$ and $p_{\perp k}/p_0 = P_{\perp k} - \tau(\phi_k - \phi_{2k})$. Note that the energy continuity equation must have a turbulent exchange term as given on the right-hand side for ion energy here:

$$\frac{\partial E}{\partial t} + \frac{\partial \Gamma_{Ex}}{\partial x} = p_0 \sum_k \left(\frac{\partial(n_k/n_0)^*}{\partial t}\right)\left(\frac{e}{T}\right)\Phi_k, \tag{14}$$

For adiabatic electrons used here, n_k and Φ_k are in phase and there is no plasma flow or exchange term. We need only concern ourselves with the ion heat flow which we summarize by quoting $\chi = \Gamma_{Ex}/(p_0/L_T)$ in gyro-Bohm units $c_s\rho_s^2/a$.

It should be noted that no special physics has been introduced to deal with the $k_y = 0$ radial modes. For these modes the ω_* terms disappear and only the geodesic curvature survives. The $k_\|$ terms tend to be small but finite. The principal damping for these modes is given by the Landau damping associated with the geodesic curvature drifts although some parallel motion Landau damping is present. Our earlier paper, Ref. 10, suggested that magnetic pumping could have some effect on the damping of radial modes. This was based on the use of neoclassical turbulence equations with time-independent viscosity.[28] This leads erroneously to damping rates $(B_\phi/B_\theta)^2 \approx 10^2$ in excess of the standard magnetic pumping drag rate on equilibrium scale poloidal rotations. When the Shaing and Hirshman[29] formulation with time-dependent viscosity is used, a much smaller poloidal rotation drag rate on the order of the ion–ion collision rate is found. This rate is too small to be of influence.

III. 3-D NONLINEAR BALLOONING MODE REPRESENTATION

Previous nonlinear ballooning mode representations (BMR) have resulted in very awkward and impractical two-dimensional (2-D) formulations of the nonlinearity which do not properly account for the third-dimension ballooning mode angle $\hat\theta$. By using the "twisted eddy basis" of Cowley et al.[9] we have formulated a simple and practical nonlinear BMR. Starting from the lab fixed basis (x,y,z) we transform to the twisted eddy basis (x',y',z'):

$$x = x',$$
$$y + \hat{s}x(z/Rq) = y', \tag{15}$$
$$z = z',$$

with

$$\frac{\partial}{\partial x} = \frac{\partial}{\partial x'} + \hat{s}\left(\frac{z'}{Rq}\right)\frac{\partial}{\partial y'},$$
$$\frac{\partial}{\partial y} = \frac{\partial}{\partial y'}, \tag{16}$$
$$\frac{\partial}{\partial z} = \frac{\partial}{\partial z'} + \hat{s}\left(\frac{x'}{Rq}\right)\frac{\partial}{\partial y'}.$$

Thus z' stays along the sheared field as radial or cross-flux surface variable x' changes $[\partial/\partial z' = \partial/\partial z - (\hat{s}/Rq)x\partial/\partial y]$ and (x',y') directions remain perpendicular to the magnetic field. Fourier transforming in the perpendicular directions from (x',y',z') to (k_x',k_y',z') we have

$$k_x = k_x' + \hat{s}(z'/Rq)k_y',$$
$$k_y = k_y', \tag{17}$$
$$z = z'.$$

Writing the curvature drift frequency as

$$\omega_D = \left(\frac{2}{R}\right)\left\{k_y' \cos\left(\frac{z'}{Rq}\right) + \left[\hat{s}\left(\frac{z'}{Rq}\right)k_y' + k_x'\right]\sin\left(\frac{z'}{Rq}\right)\right\}$$
$$= \left(\frac{2}{R}\right)\left(\frac{nq}{r}\right)[\cos(\theta) + \hat{s}(\theta - \hat\theta)\sin(\theta)], \tag{18}$$

it is easy to identify the (k_x',k_y',z') basis with the usual BMR:

$$k_y' = k_\theta = (nq/r) \tag{19}$$

is the good quantum number toroidal label n with q and r the safety factor and radius of the reference flux surface,
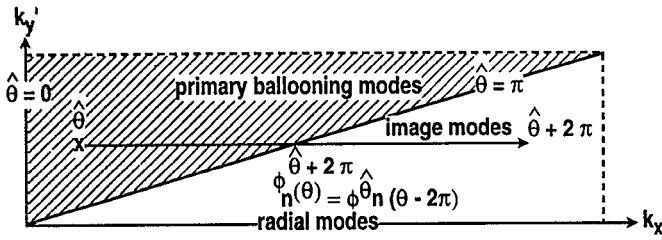
$$z'/Rq = \theta \tag{20}$$

FIG. 1. Ballooning mode and radial mode grid in (k_x', k_y').

is the extended poloidal angle along the field line, and

$$-k_x'/k_y'\hat{s} = \hat{\theta} \tag{21}$$

is the ballooning angle or phase between poloidal harmonics starting at a reference rational surface $m = nq$. The gradient parallel to the field line is

$$ik_{\parallel} = \frac{\partial}{\partial z'} = \left(\frac{1}{Rq}\right)\frac{\partial}{\partial \theta}. \tag{22}$$

Note that we have not included variations of shear along the field line, but consider only on concentric circular equilibria approximating very low β. Conversion of the nonlinear BMR to magnetic flux coordinates for general geometry is straightforward and will be treated in a future publication.

A crucial point emphasized in Ref. 9 is that the nonlinear convolution has a simple invariant form in the twisted eddy basis:

$$\frac{df_{k'}(z')}{dt} = \frac{\partial f_{k'}(z')}{\partial t} - \sum_{k_1'}(k_{x1}'k_{y2}' - k_{x2}'k_{y1}')$$
$$\times \phi_{k_1'}(z')f_{k_2'}(z'), \tag{23}$$

with $\mathbf{k}_2' = \mathbf{k}' - \mathbf{k}_1'$.

Fourier amplitudes in the transformed twisted eddy basis (k_x', k_y', z') as they stand are not periodic in the physical poloidal angle. To impose periodicity, it is convenient to distinguish "primary" modes and "image" modes. Linear mode labels are given by $(n, \hat{\theta})$ or (k_y', k_x'). The linear modes will be centered about $\theta = \hat{\theta}$, with $\hat{\theta}$ near 0 ballooning in the bad curvature region and $\hat{\theta}$ near π in the good curvature region. Primary modes have $-\pi < \hat{\theta} \leq \pi$. Each primary mode has an infinite series of image modes labeled by $-\infty < p < \infty$ with the same n (or $k_{y'}$) but with $\hat{\theta} \rightarrow \hat{\theta} + p2\pi$ [or $k_{x'} = k_{x'} + p\hat{s}k_{y'}(2\pi)$] (see Fig. 1). As linear modes, the image modes have the same linear growth rate as the primary except they are centered about $\theta \rightarrow \theta + p2\pi$. On an infinite grid, the statistical or time average of intensity of the image modes must be identical θ displaced copies of the primaries. Imposing instantaneous cyclic symmetry of the images with the primaries as in the original BMR[30] for any field F,

$$F_n^{\hat{\theta}+2\pi p}(\theta) = \exp(-ip2\pi nq)F_n^{\hat{\theta}}(\theta - 2\pi p), \tag{24}$$

or equivalently,

$$F_{k_{x'}+2\pi p\hat{s}k_{y'},k_{y'}}(z')$$
$$= \exp(-ip2\pi nq)F_{k_{x'},k_{y'}}(z' - 2\pi pRq),$$

preserves 2π periodicity of amplitudes poloidally (as well as toroidally). From $y = r(\theta - \phi/q)$ it is easy to reconstruct the real space physical perturbations periodic in θ and ϕ as

$$F(x,\theta,\phi) = \sum_p \sum_n \int_{-\pi}^{\pi}\left(\frac{d\hat{\theta}}{2\pi}\right)\exp\left[-in\phi + inq\right.$$

$$\times (\theta - p2\pi) + inq\hat{s}(\theta - p2\pi - \hat{\theta})\left(\frac{x}{r}\right)\right]$$

$$\times F_n^{\hat{\theta}}(\theta - 2\pi p) + \sum_{k_x} F_0^{k_x}(\theta)\exp(ik_x x), \tag{25}$$

where $\sum_p\sum_n\int_{-\pi}^{\pi}(d\hat{\theta}/2\pi)$ and $\sum_{k_x'}\sum_{k_y'}$ are used interchangeably. Included in this summation over finite-n ballooning modes are the $n = 0$ (or $k_y' = 0$) radial modes having $k_x' \neq 0$ which we discussed in the Introduction. They are explicitly periodic with $F_0^{k_x}(\theta) = F_0^{k_x}(\theta + 2\pi)$. We clairify at this point that $k_y' = 0$, $k_x' = 0$ is not a time-evolved "mode" but rather the equilibrium. Space and time scale separations are implicit in our discussion. The long space scale equilibrium evolves on a long time scale by a transport equation, e.g., Eq. (14), containing energy sources. The local equilibrium gradients ultimately determined from the transport equation are assumed to be in steady state here.

The plasma energy flow at poloidal angle θ, for example, is given by the time average $\langle\ \rangle$,

$$\Gamma_{Ex}(\theta) = \frac{3}{2}p_0\sum_p\sum_n\int_{-\pi}^{\pi}\left(\frac{d\hat{\theta}}{2\pi}\right)\left\langle\left(\frac{p^a}{p_0}\right)_n^{*\hat{\theta}}(\theta - 2\pi p)\right.$$

$$\times\left(\frac{-i(nq/r)c\Phi_n^{\hat{\theta}}(\theta - 2\pi p)}{B}\right)\right\rangle. \tag{26}$$

Cowley et al.[9] advocate forgoing amplitude periodicity. This amounts to advancing the image modes independent of the primaries. They argue that sufficiently short correlation length along the field line makes periodicity of amplitudes irrelevant. This indeed may be the case. However, practically we must numerically truncate the grid in θ and $\hat{\theta}$ (as well as n) and the periodicity condition Eq. (24) affords a convenient way of doing this. What must be avoided is advancing a ballooning mode (or image mode) forcing a zero or periodic boundary condition at the grid boundaries $\theta = \theta_{min}$ or $\theta = \theta_{max}$. There are at least two ways to do this.

If the turbulence is sufficiently ballooning, the primaries can be advanced on $-2\pi = \theta_{min} \leq \theta < \theta_{max} = 2\pi$ with nonlinear coupling only to nearest neighbor images $p = +1$ and $p = -1$ as θ displaced cyclic copies. In effect the nonlinear coupling grid ($\mathbf{k}_1'$ and $\mathbf{k}_2'$) extends only from $-3\pi < \hat{\theta} \leq 3\pi$ with $\mathbf{k}$ restricted to $-\pi < \hat{\theta} \leq \pi$. No other coupling is possible since only these images overlap in θ with the primaries. It is possible to show that for $-2\pi < \theta < 2\pi$, this is an energy conserving procedure. Defining the system primary "energy" from $\theta_{min} \leq \theta < \theta_{max}$ and $\mathbf{k}$ within $-\pi < \hat{\theta} \leq \pi$ as $E = (1/2)\int d\theta\sum_k\sum_i f_k^{i*}(\theta)f_k^i(\theta)$ with $i = 1,4$ denoting the four time advanced moment fields, then energy enters and leaves the system only linearly with the nonlinear terms only pass-

ing energy from one mode to another. Energy is passed non-linearly from one θ location to another only by interaction of the primaries with the images (i.e., retaining only primaries with no interaction with images nonlinearly preserves energy at each θ). The *a posteriori* validity condition is that the primary mode amplitudes are sufficiently small near the boundaries at $\theta = \pm 2\pi$. For very strong ballooning it may be sufficient to ignore coupling to the images entirely. Of course if the turbulence becomes interchange-like extending to θ well beyond $\pm 2\pi$ and requiring $p = \pm 2$ and so on, the method becomes impractical. This approach was used in Ref. 10. It has the advantage that the resulting turbulence is exactly periodic. It proves to have several disadvantages. The high-n or high-k_y $p = \pm 1$ images are very small in amplitude yet they have a very high $k_{x'}$ and determine the Courant numerical stability condition on the time step

$$\Delta t \lesssim \min\{1/(k_{x\_\max}\bar{V}_{Ex}), 1/(k_{y\_\max}\bar{V}_{Ey})\}.$$

The low-n $p = \pm 2$ images do start to overlap with the primaries but they cannot be included without further increasing $k_{k\_\max}$.

A much more practical scheme has been invented by Beer et al.[11] The (k_x', k_y') grid has a simple rectangular truncation. Many low-k_y (low-n) images are retained and few if any of the less important high k_y. It should even work at least to some extent if the modes start to become interchange-like. The truncation of the θ grid and imposition of its boundary conditions are unique. The θ grid is divided into a "physical box" $-\pi \leqslant \theta < \pi$ with "right and left extensions" $\theta_{\min} \leqslant \theta < -\pi$ and $\pi \leqslant \theta < \theta_{\max}$. (We take $\theta_{\min} = -2\pi$ and $\theta_{\max} = 2\pi$ although this is somewhat arbitrary.) At each time step each $(k_x' k_y')$ is advanced in time over the whole extended box with no distinction between primaries and images. At the end of each time step, the information in the right and left extensions is "thrown away." It is replaced by information (i.e., field amplitudes) within the physical box using the cyclic condition Eq. (24) and shifting θ as needed. Technically this leads to a discontinuity of amplitudes at $\theta = \pm \pi$ but this quickly "anneals" and in effect smooth boundary conditions on the physical box are provided. Turbulent energy summing over all $(k_x' k_y')$ within the physical box is well conserved in practice. The radial modes can be advanced with 2π periodicity enforced exactly and directly or they can be advanced freely over the extended box. Since the total of the driving ballooning modes are nearly 2π periodic the radial modes become nearly periodic. A small disadvantage of the method is that if the k_x' grid is too small, then the diffusion over the full box is not quite periodic. In fact $\chi(2\pi)$ differing substantially from $\chi(0)$ is a signature that more k_x' modes should be kept.

We note in passing that the Fourier representation in k_x and k_y is particularly convenient for exact evaluation of the Bessel function forms and the toroidal dissipative terms with $|\omega_D|$. In fact advancement of the parallel gradient terms, and in particular the dissipative terms with $|k_\parallel|$, is most easily done by a "time-split" algorithm Fourier transform from θ to $k_\parallel$ space.

IV. EQUILIBRIUM SCALE SHEARED ROTATIONAL FLOWS

The BMR as presented here is a Fourier transform representation which intrinsically assumes that the turbulence is homogeneous from one flux surface to another or that the correlation length is shorter than any equilibrium length scale. Profile effects or gradual inhomogeneities are generally ρ_s/a small and ignorable. The exceptions are when the plasma is spun-up to have large equilibrium potentials $e\Phi/T_e \gg 1$ or when sharp gradients in the radial electric field build up near the edge. In either case the equilibrium sheared flow rate cE_x'/B can become comparable to the mode growth rates $\gamma_k(k_x/k_y)$.[20] Homogeneity is broken. However, it is possible to include these linear inhomogeneities in the BMR formalism. The time derivative in Eq. (11) merely acquires a linear mode coupling term from the $\mathbf{E} \times \mathbf{B}$ shear:

$$\frac{\partial f_{ky'kx'}(\theta)}{\partial t} \rightarrow \frac{\partial f_{ky'kx'}(\theta)}{\partial t} + \gamma_E k_{y'} \frac{\partial f_{ky'kx'}(\theta)}{\partial k_{x'}}, \quad (27)$$

where $\gamma_E = [(cE_x'/B)/(c_s/a)]$ is the shear rate for $\mathbf{E} \times \mathbf{B}$ motion in normalized units. (We have simply replaced the $x = x'$ variation in the $\mathbf{E} \times \mathbf{B}$ flow with $-i\partial/\partial k_x'$.)

The label k_x' is no longer a good linear quantum number for normal modes of the system. However, the interpretation of normal mode stability is dependent on whether k_x' in Eq. (27) is regarded as a continuum variable or a discrete variable as discussed in a recent paper by Miller and Waltz.[31] If k_x' is continuous, then in x space the "box" over which there is constant shear extends to infinity (or if finite includes an infinite number of singular surfaces per n label). For normal modes a transformation of variables can be made in which $\hat{\theta}$ is replaced by $\hat{\theta}_0 + (\gamma_E/\hat{s})t$. No matter how weak the rotational shear a mode ballooning at $\theta = \hat{\theta}_0$ will slowly convect in θ (or $\hat{\theta}$) sampling all ballooning angles passing through regions of good and bad curvature. The eigenmodes in this picture have a time average growth rate $\gamma_{ave} = \int_{-\pi}^{\pi}(d\hat{\theta}/2\pi)\gamma_0(\hat{\theta})$ where $\gamma_0(\hat{\theta})$ is the normal mode rate in the absence of rotational shear.[32] Such "continuum" eigenmodes may be a meaningless representation of system stability not only because the system is not infinite in x space but also because at very weak shear such eigenmodes could not be formed in a turbulent decorrelation time (or in other words, the number of linear exponentiations over a formation period could be huge).

On the other hand, if k_x' is discrete corresponding to a finite box in x space, the most unstable eigenmodes have growth rates at weak shear only slightly depressed from the unsheared normal mode rates. These modes, however, are formed at the "edge" of the box whereas the more stable continuum-like modes live at the center of the box. At sufficiently large rotational shear the edge modes become continuum modes independent of the box length.[31] Here we use discrete k_x' corresponding to a finite x-space box with cyclic boundary condition to model homogeneous turbulence. A key validity condition is that the turbulence in the presence of the rotational shear must appear homogeneous with no preference for the edge of the box. In effect we represent equilibrium sheared electric fields on the same basis as non-

linearly generated fields. There is an additional technical consideration when treating k_x' as a discrete variable missed in Ref. 10. A three-point derivative must not be used. In fact it corresponds to a sinusoidal rotational velocity profile in x space with points of vanishing rotational shear. A constant rotational shear profile is represented in k_x' by a harmonic derivative[31]

$$\frac{\partial f_k}{\partial k_x'} \rightarrow \sum_{m \neq 0} \left(\frac{1}{m}\right)(-1)^{m+1}(f_{k_y', k_x' + m\Delta k_x'}$$

$$-f_{k_y', k_x' - m\Delta k_x'})/\Delta k_x'. \tag{28}$$

In the center of the tokamak, plasma rotations of interesting strength are actually almost purely toroidal. Poloidal rotations are no larger than diamagnetic and their shear rates are usually far from comparable to linear mode growth rates hence ignorable. Thus we should consider $E \times B$ sheared rotation in combination with parallel sheared velocity flow consistent with purely toroidal rotation. Parallel sheared flow contributes to the stabilizing Doppler shift variation as does $E \times B$ flow[33] and it contributes to a Kelvin–Helmholtz destabilization (see Ref. 34 for example). For sheared parallel flow, the term $- i\gamma_P k_y' \phi_{1k}$ must be added to the right-hand side of Eq. (2) where $\gamma_P = V_\parallel'/(c_s/a)$ is the parallel shear flow rate. For purely toroidal rotation the poloidal projections of the parallel velocity and the $E \times B$ velocity must cancel. It is straightforward to show that the total Doppler shift rotational shear rate including the parallel shear velocity effect is actually $\gamma_E = (r/q)[d(V_\phi/R)/dr]/(c_s/a)$ instead of the purely $E \times B$ shear flow rate $d(rV_\phi/qR)/dr = (cE_x'/B)$ and further the parallel shear drive is $\gamma_P \approx (dV_\phi/dr)/(c_s/a)$. Thus for purely toroidal sheared flow $\gamma_P \approx (Rq/r)\gamma_E$.

V. NUMERICAL ILLUSTRATIONS

A. Standard case

The numerical illustrations presented here are organized around a toroidal standard case with physical parameters $R/a = 3$, $a/L_n = 1$, $a/L_T = 3$, $\tau^{-1} = T_i/T_e = 1$, $q = 2$, and $\hat{s} = 1$. The parameters are meant to be typical of $r/a = 0.5$. The numerical parameters are $(nq/r)_{-max} \rho_s = k_{\theta\_max}\rho_s = 1$ or in normalized units $k_{y\_max}' = 1$, with $\Delta k_y' = 0.1$, $k_{x\_max}' = \hat{s}k_{y\_max}'\pi$, and $\Delta k_x' = (\hat{s}\pi/4)\Delta k_y' = 0.078$. This spans 850 complex modes including all primary ballooning modes ($p = 0$) with $-\pi \leqslant \hat{\theta} \leqslant \pi$, many image modes and radial modes. There are 10 modes on the positive k_y' axis and 40 on the positive k_x' axis; we will refer to a $10k_y \times 40k_x$ quadrant (see Fig. 1) The grid along the field line spans the extended box $-2\pi < \theta < 2\pi$ with $\Delta\theta = 4\pi/64$. A small artificial viscous damping rate $\mu_x k_x^2$ with $\mu_x = 0.05$ is put on the fields. A typical time step is $0.05(c_s/a)$ and good statistical averages appear to require run times of order $800(c_s/a)$.

This mode spacing is relatively coarse but adequate. Here, ρ_s/a which determines the maximum toroidal n number simulated does not enter the calculation. However, to put this grid density in perspective, if $\rho_s/r = 0.0025$ then the maximum physical (m,n) is $(400,200)$. If $\Delta k_y'/k_{y\_max}'$
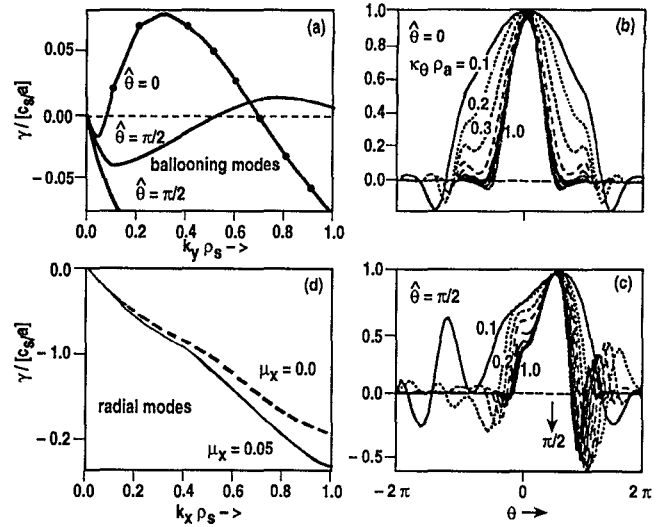

FIG. 2. Linear ballooning mode growth rate spectrum (a); extended angle q mode structure for $\hat{\theta} = 0$ (b), and $\hat{\theta} = \pi/2$ (c); radial mode damping spectrum (d) for standard case.

$= 1/10$ this implies that Δn is 20. This corresponds to simulating $1/20$ of the torus or a field line following tube in the flux surface of toroidal outboard midplane intersection width $\Delta\phi = 2\pi/20$, perpendicular width $\Delta y = \Delta\phi r/q$ in the flux surface, and thickness across the flux surface $\Delta x = \Delta y(4/\hat{s}\pi) = 0.2r$ or $80\rho_s$. In effect the cross-field correlation lengths are assumed to be shorter than this band width and thickness.

Figure 2 illustrates the linear growth rate spectrum and normal ballooning mode structure at various $\hat{\theta}$ for the standard case. The maximum growth rate is 0.083 at $k_y' = 0.3$ and $\hat{\theta} = 0$ [Fig. 2(a)]. The mode frequency increases roughly linearly with k_y' having a value of -0.28 at $k_y' = 0.3$. It is readily apparent that modes with $\hat{\theta}$ beyond $\pi/2$ are damped and that as expected, modes are localized about $\theta = \hat{\theta}$ [Fig. 2(c)]. The lower k_y' modes have an increasingly wider extent along the field line [Fig. 2(b)]. Modes at $\hat{\theta} = 0$ with $k_y' < 0.1$ appear to go stable at $k_y' < 0.07$ with damping rates of -0.02 at $k_y' = 0.04$. (These are not included in the standard case simulation but do appear in simulations at much smaller $\Delta k_y'/k_{y\_max}'$.) We have found no evidence of low-k_y' unstable interchange-like modes extending over many (10's) 2π.

The linear growth rates and mode widths from four-moment GLF models compare reasonably well with the kinetic theory calculations although not as well as may have been expected from the excellent agreement in local kinetic theory.[4] Using Kotschenreuther's initial value gyrokinetic code[35] the simple gyroaverage GLF model peak growth rate γ_{max} is 0.89, the kinetic value and its mixing length $\Delta_x = 1/(\hat{s}k_y\theta_{RMS})$ is 0.82 of the kinetic value; thus the relative mixing length diffusion $D_{ML} = \gamma_{max}\Delta_x^2$ is 0.6 the kinetic value. [Recall that a linear mixing length $\Delta_x = 1/(\hat{s}k_y\theta_{RMS})$ corresponds to the characteristic radial width of a poloidal harmonic when a single ballooning mode is transformed back to the (m,n,r) representation. The phasing between adjacent poloidal harmonics corresponds to the ballooning angle $\hat{\theta}$ in this picture.] The critical gradient is $a/L_T = 1.8$
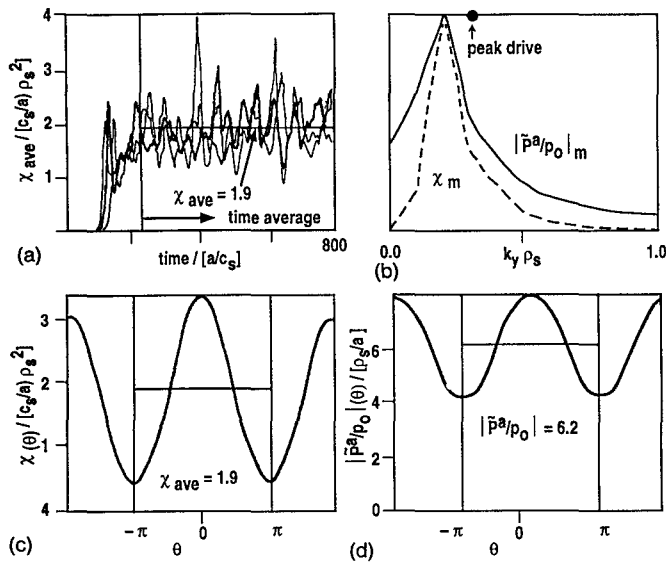
FIG. 3. Standard case nonlinear simulation. (a) Ensemble of traces for flux surface average diffusivity versus time; (b) pressure perturbation and diffusivity spectrum at $\theta=0$ versus poloidal wave number; (c) time average diffusivity versus extended poloidal angle θ; (d) time average pressure perturbation versus extended poloidal angle θ.

FIG. 4. Instantaneous density fluctuations for each k_x' for several k_y' versus extended poloidal angle in standard case. Upper right-hand panel shows comparative potential fluctuations for radial modes.

whereas the kinetic value is 1.4. In general there is considerable improvement going to six field models.[12] The radial mode damping rates with and without the artificial damping is shown in Fig. 2(d). Unfortunately we presently have no comparison with kinetic theory for these modes.

Figure 3 illustrates the nonlinear simulation of the standard case. Figure 3(a) shows three time history traces of the flux surface average heat diffusivity χ from runs with slightly different initial conditions. All have time average values of $\chi=1.9c_s\rho_s^2/a$. In each trace there is an RMS deviation typically 1.9 ± 0.4. We do not attempt to analyze the physical significance, if any, of these statistical fluctuations in the flow. They are not reflective of the uncertainty in the time averages since the average from different realizations differs by only a few percent. In general it should be noted that there is absolutely no correlation between the instantaneous diffusivity at first maximum and the time average after it has settled into a fully saturated state. Sometimes the first maximum is much smaller and other times it is considerably larger. The spectrum of pressure perturbations and contributions to diffusion at $\theta=0$ are shown in Fig. 3(b) with peaks at $k_{y'}=0.2$ which downshifted from the peak growth rate at $k_{y'}=0.3$. The diffusion and turbulence level as a function or poloidal angle θ are shown in Figs. 3(c) and 3(d), respectively. The small deviations from $\chi(\pm2\pi)=\chi(0)$ are due to imperfect periodicity from not keeping all images. The diffusion is highly asymmetrical with an out/in ratio of 8/1 and the turbulence level is less asymmetrical at 2/1. The RMS spectral flux surface average $|\tilde{p}^a|/p_0=(6.2\pm0.7)\rho_s/a$ with outboard values $(|\tilde{p}^a|/p_0)(0)=8.0\rho_s/a$ and $(|\tilde{n}|/n_0)(0)=6.5\rho_s/a$.

There are several ways to present the detailed spectrum for the turbulence. Figure 4 shows an instantaneous plot of the density perturbations $[|\tilde{n}_{k_y,k_x}(\theta)|/n_0]/(\rho_s/a)$ along the
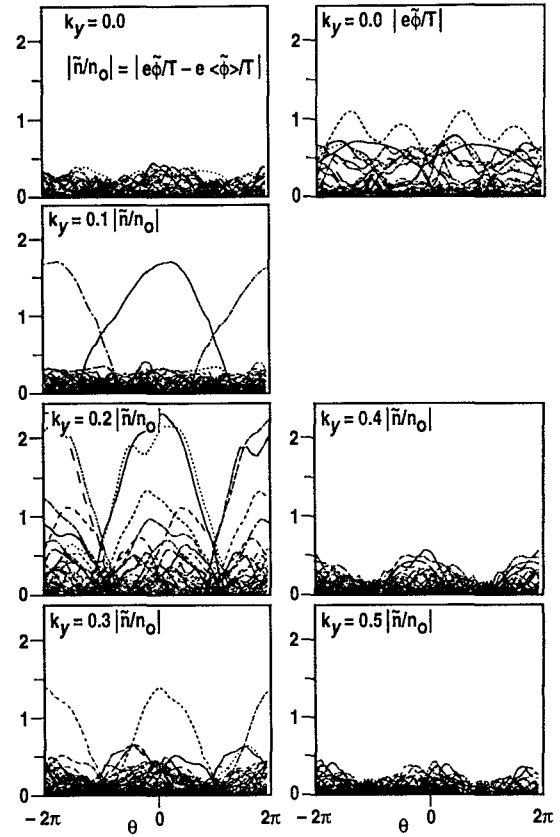
field line for each k_x' in each k_y' from 0.0 to 0.5 (ignoring the smaller spectra for 0.6 to 1.0). The image modes for the larger amplitude ballooning modes are clearly visible. Clearly the overlap of images with primaries is small in this case. For radial modes at $k_y' = 0$ we also show the spectrum of $|e\Phi_{0,k_x}/T_e|/(\rho_s/a)$ to indicate the importance of subtracting away the flux surface average potential.

Figure 5 shows a color contour plot of the instantaneous $\tilde{n}/n_0$ projecting the ballooning mode representation back to real space. This is a constant toroidal angle annular plot made by stacking intersections of identical copies of the field line following tube which is the actual simulation box (see the above discussion of the tube dimensions $\Delta x, \Delta y$). This particular plot was made from a simulation at double the k_x' grid density from the standard case so that the width of the annulus is $\Delta x=160\rho_s$ rather than $80\rho_s$ as in the standard case. Using $r/a=0.5$ the aspect ratio of the annulus (minor radius to width) specifies a specific ρ_s/a chosen only for convenience of display to make the eddies visible. (In this case the aspect ratio for the annulus $\Delta x/r\approx1$ making $\rho_s/a\approx0.003$, which is not more than two times typical values. See the discussion of TFTR cases in Sec. V D.) The red (blue) portions represent high and low density and potential with co- and counterclockwise cyclonic motions. These eddies are most vigorous on the outboard low field side. There is some tendency for the radially elongated eddies to line up
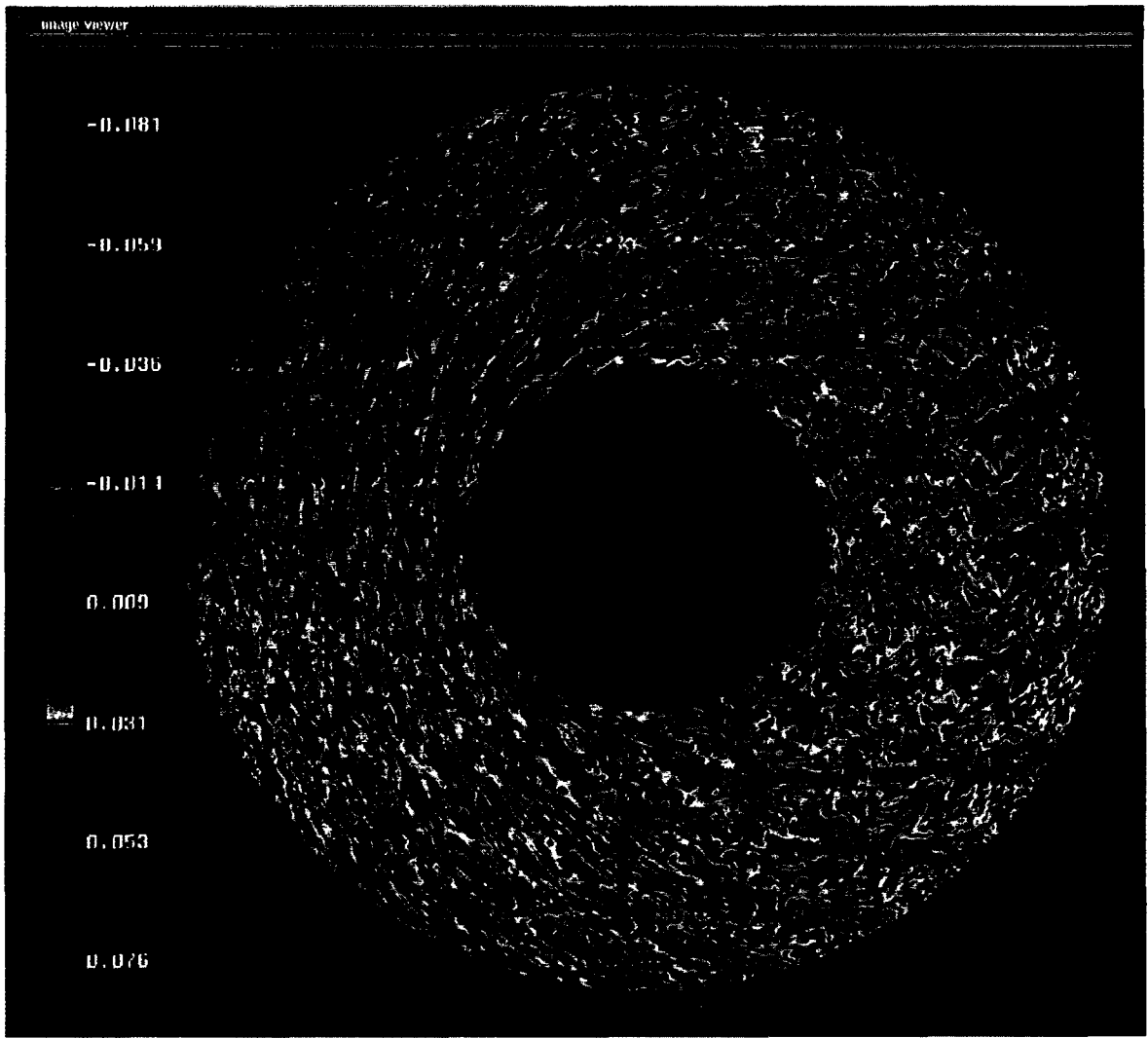
FIG. 5. Instantaneous density contour plots on a constant toroidal angle radial annulus formed by eight intersections with simulation band for the standard case.

as "streamers"[36] but we believe the correlation lengths are effectively less than half the radial width. The standard case simulations for a box (or annulus) $80\rho_s$ wide have nearly the same transport, turbulence level, and the time-averaged k-space average spectrum as for a box $160\rho_s$ wide which means that there are an adequate number of radial correlation lengths in the box for the assumed cyclic symmetry (i.e., any eddy leaving the right side will enter the left side of the annulus). We hasten to point out, however, that the even for an aspect ratio of $\Delta x/r \approx 1/2$ and $\rho_s/a \approx 0.0015$ the eddies appear to be rather large and we should expect some convection of the turbulent energy from the box because of inhomogeneity in the turbulence and gradient profiles over the scale of the eddies. Convection of turbulent energy from the box (not just through the box) is outside the scope of the BMR presented here and requires a radially global simulation to quantify. The BMR simulations effectively operate at vanishing ρ_s/a.

The k-space spectrum for the standard case is shown in Fig. 6. The complete contour map of the (k_y',k_x') spectrum of

time averaged $|\tilde{n}/n_0|$ at $\theta=0$ is shown in Fig. 6(a). The peak is a $(k_y',k_x') = (0.2,0.0)$ downshifted from the peak drive at $(0.3,0.0)$. Clearly, there is less action in the region of image modes but the radial modes are a significant part of the spectrum. Figure 6(b) plots the RMS integrated spectra $|\tilde{n}_{k_y}|/n_0 = [\Sigma_{k_x}(|\tilde{n}_{k_y,k_x}|/n_0)^2]^{1/2}$ and $|\tilde{n}_{k_x}|/n_0 = [\Sigma_{k_y}(|\tilde{n}_{k_y,k_x}|/n_0)^2]^{1/2}$ along with the radial mode spectrum $|n_{0,k_x}|/n_0$. Note that the radial mode spectrum does not condense or peak at the longest wave number of the simulation but rather has a broad maximum at intermediate wave numbers. (The appearance of two maxima in this particular case is not general and not significant.) The nonvanishing $k_y \to 0$ portion of $|\tilde{n}_{k_y}|/n_0$ in comparison to the peak is the best observable signature of radial modes. The radial mode signature, the peak in the RMS integrated spectrum $|\tilde{n}_{k_y}|/n_0$ near $k_y \approx 0.2$, and the peak in RMS integrated spectrum $|\tilde{n}_{k_x}|/n_0$ near $k_x = 0$ are in rough agreement with BES spectral plots for core turbulence in TFTR[37] as has been previously reported for gyrokinetic toroidal simulations.[8]
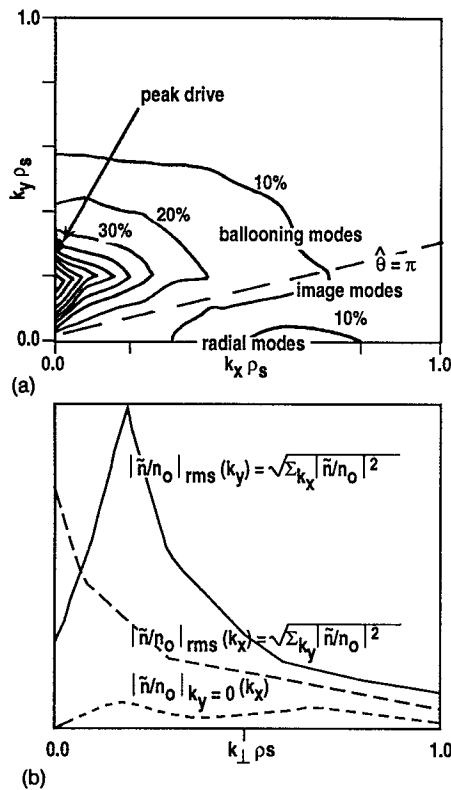
FIG. 6. (k_y, k_x) time average spectrum of density fluctuation in 10% incremental contours (a) RMS integrated k_y' spectrum, RMS integrated k_x spectrum, and k_x spectrum of radial modes (b).

These are at least in part likely to be general features of toroidal turbulence. However, caution is advised in comparing details since beam emission spectroscopy (BES) spectra at larger radii do not appear to have a significant radial mode content.[37]

The most dramatic demonstration of the importance of radial modes is to compare with simulations containing only primary ballooning modes. As shown in Table I, *retaining radial modes reduces transport almost tenfold*. The reduction is caused almost entirely by the radial modes. Runs with primary ballooning modes retaining images but no radial modes have initially the same transport levels as primaries alone but slowly drift away without long term saturation. The toroidal curvature drive is the dominant destabilizing mechanism for ITG turbulence. *A "slab" ITG simulation turning off the curvature has twentyfold less transport than the toroidal simulation* and again including radial modes gives a tenfold reduction.

We have made several numerical fidelity checks. For example, doubling the θ grid density from 64 to 128, or changing the boundary conditions from zero at $\theta = \pm 2\pi$ to periodic

TABLE I. Toroidal and slab simulations with/without radial modes.

	Torus radial	Torus	Slab radial	Slab
$\chi/(c_s \rho_s^2/a)$	1.9	17	0.087	0.5
$|\tilde{p}^a/p_0|/(\rho_s/a)$	6.2	18.8	1.2	3.5

on $-2\pi < \theta < 2\pi$ has little effect. Energy conservation is carefully monitored at each time step. The typical time step is $0.05a/c_s$ but halving the time step does not change the result.

Overall there is a remarkable insensitivity to threefold changes in (k_y', k_x') grid density and twofold changes in k_{y_max}' and k_{x_max}'. Table II shows almost complete invariance to $\Delta k_x'$. There is at worst a 40% increase in χ with a threefold decrease in $\Delta k_x'$. A twofold decrease in k_{y_max}' shows an improperly truncated k_y' grid spectrum but even this extreme changes χ by only 40%. Removing the artificial viscosity in the k_x direction decreases the diffusion by about 15%. This is likely because the radial modes are less damped and cause more reduction in the ballooning mode transport.

Our conclusion is that *the relative insensitivity to drastic changes in the gyronormalized grid suggests that gyro-Bohm scaling $\chi \propto c_s \rho_s^2/a$ is operative for these simulations*. In the BMR representation as presented the relative gyroradius ρ_s/a parameter does not explicitly enter the gyronormalized grid. This parameter can enter only via small "profile" variations terms (e.g., variations in temperature gradients) which have been explicitly dropped, radial convective loss of turbulent energy not allowed by the Fourier representation, or grid density and truncation. Only the latter can be tested. The gyronormalized (k_y', k_x') grid behaves as a continuum and there is no evidence that the peak in the spectrum changes with grid density.

B. Effect of sheared rotational flows

As we noted in Sec. IV for purely toroidal drive consistent with a core plasma, the attendant parallel shear rate γ_P destabilizes the ITG mode and combined with the $\mathbf{E} \times \mathbf{B}$ to cancel the poloidal rotation, gives a stabilizing Doppler shear rate $\gamma_E = (r/Rq)\gamma_P$. Figure 7(a) shows the spectrum of most unstable outward ballooning modes in the presence of parallel shear. Figure 7(b) shows the effect of the Doppler shear with and without the corresponding parallel shear at $Rq/r = 12$ and 18 for the standard case. We find that *the transport can be made to vanish for a critical Doppler shear rate with $\gamma_E \approx \gamma_{max}$*. For example, for $\gamma_P = 0$, the critical $\gamma_E = 0.07$ whereas $\gamma_{max} = 0.083$. We have not made an exhaustive parametric test of this rule but, for example, at $a/L_T = 4$, the critical $\gamma_E = 0.18$ and $\gamma_{max} = 0.18$. Even for the case of vanishing magnetic shear which we discuss in Sec. V C, the critical γ_E and γ_{max} are very close. This is somewhat surprising since it could be argued the critical shear rate occurs when the maximum growth rate of the most unstable ballooning mode becomes less than the convection rate for the ballooning mode angle going from the unstable outward ballooning point $\theta_0 = \pi$ to the stable inward ballooning point $\theta_0 = \pi$. (See the discussion in Sec. IV about rotational shear and convection in ballooning angle.) However $\gamma_E \approx \pi \hat{s} \gamma_{max}$ does not describe the vanishing magnetic shear case. More work is needed to verify that our rule $\gamma_E \approx \gamma_{max}$ has no other parametric factors. From Fig. 7(b) it is apparent that at low current (high q or high Rq/r) the stabilizing Doppler shear may not keep up with the destabilizing effect of the corresponding γ_P. For example, at $\gamma_P = 1.2$, $\gamma_E \geq 0.1$ is needed.

TABLE II. Variation of (k_x',k_y') grid density and cutoff $\hat\theta_{max}=\pi$ fixed.

	$10k_y\times30k_x$	$10k_y\times40k_{x_-}$ STD	$10k_y\times80k_x$	$10k_y\times30k_x$ (0.5)
$\chi/(c_s\rho_s^2/a)$	1.85	1.9	1.88	2.66
$|\tilde{p}^a/p_0|/(\rho_s/a)$	5.92	6.24	5.92	7.63
	$10k_y\times40k_{x_-}$ STD	$20k_y\times40k_x$	$30k_y\times30k_x$	$10k_y\times40k_{y_-}\mu=0$
$\chi/(c_s\rho_s^2/a)$	1.9	2.45	2.66	1.6
$|\tilde{p}^a/p_0|/(\rho_s/a)$	6.24	7.45	7.7	5.9

The $Rq/r=12$ curve cannot reach complete stabilization, even though there is a dramatic reduction in transport at modest shear rate.

The linear destabilizing effect of parallel shear on γ_{max} is in general easy to calculate even in more elaborate toroidal models. The Doppler stabilizing effect is not easily calculated even linearly for toroidal geometry. However, if the above rule for critical Doppler shear $\gamma_E\approx\gamma_{max}$ is generally valid, then we would have an easy way to assess rotational effects. Note that the critical $\gamma_E\approx\gamma_{max}$ results from a simple balance of terms in Eq. (27) $\gamma_E=\gamma_k(k_x/k_y)$ and given that average decorrelation rates $\Delta\omega\approx\gamma_{max}$, there is not much difference [at least for an isotropic spectrum with $(k_x/k_y)\approx1$] with the Biglari, Terry, and Diamond rule[20] $\Delta\omega/(k_y\Delta x)$ except that decorrelation rates $\Delta\omega$ and width Δx are not easily estimated.
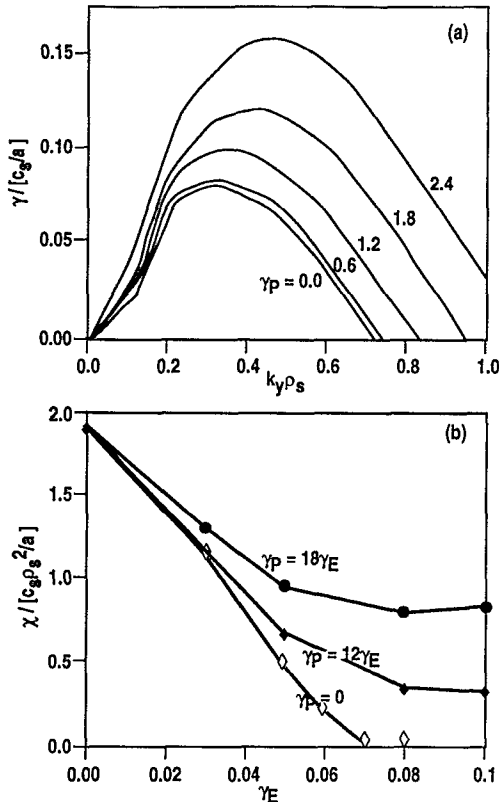

FIG. 7. Standard case spectrum of unstable ITG modes driven by parallel shear flow (a); ITG transport versus Doppler shear rate with and without parallel shear destabilization consistent with purely toroidal rotation (b).

An important experimental signature of the Doppler shear stabilization effect is the $k_x=k_x'$ asymmetry it produces in the spectrum at $\theta=0$. For the standard case, with $\gamma_E=0.05$, $\gamma_P=0.6$, the peak $(k_{y'},k_{x'})=(\pm0.3,\pm0.2)$ at $\theta=0$. There is a corresponding up–down asymmetry in the turbulence which peaks near $\theta=0.7$ rad suggested by $\hat\theta=k_x'/(k_x'\hat{s})$. Using Eq. (17), this means that the spectrum measures at $\theta=0.7$ will have no k_x asymmetry. The contour density plot for $\gamma_E=0.06$ and $\gamma_P=0$ is shown in Fig. 8 in the same perspective as the no rotational shear case Fig. 5. The eddies are sheared and diminished in size. The shearing angle lines up with $\hat\theta=k_x'/(k_x'\hat{s})=0.7$.

As a technical point it should be noted that the results are insensitive within some limits as to how many terms are kept in the harmonic derivative in Eq. (28). Terms up to ±5 and ±10 give the same result as keeping all. It is important to use the harmonic derivative. A three-point centered derivative requires a Doppler shear several times larger because, as we have noted, it corresponds to a sinusoidal rotational profile with half the average RMS shear. It also produces no asymmetry in the spectrum since both signs of rotational shear are present in a sinusoidal profile. We have also done simulations by directly imposing a linear Doppler shear profile in real space, then transforming back to k_x' space. These methods prove to the equivalent.

C. Parametric variation of toroidal ITG transport

The critical a/L_T for the parameters of the standard case is 1.8. We have seen no evidence of subcritical turbulence. The transport is generally described by $\chi\propto(c_s/R)\rho_s^2 F(R/L_T,R/L_n,q,\hat{s})$ assuming gyro-Bohm scaling which we believe is established in these simulations. Note that in slab geometry R, q, and $\hat{s}$ can scale only in the combination $L_s=Rq/\hat{s}$. In toroidal geometry they are separate parameters making the parametric dependence difficult to map. In the weak density gradient limit (roughly $R/L_n<3$), and near threshold, $F\propto(R/L_T-R/L_{T\_crit})$. A persistent research goal is to characterize the dependence on the remaining parameters particularly q and $\hat{s}$. Maximum linear growth rates γ_{max} and the mixing length model diffusions D_{ML} defined above may offer some guide. Figure 9 shows variations of γ_{max} and D_{ML} about the standard case at $a/L_T=3$ (as well as 4). [Note the mixing length can be inferred from $\Delta_x=(D_{ML}/\gamma_{max})^{1/2}$.] The top panels verify that $R/L_n=3$ is already in the weak density gradient regime. The bottom two panels show that the dependence on q and $\hat{s}$ is only roughly characterized by power-law dependence. Scaling away from
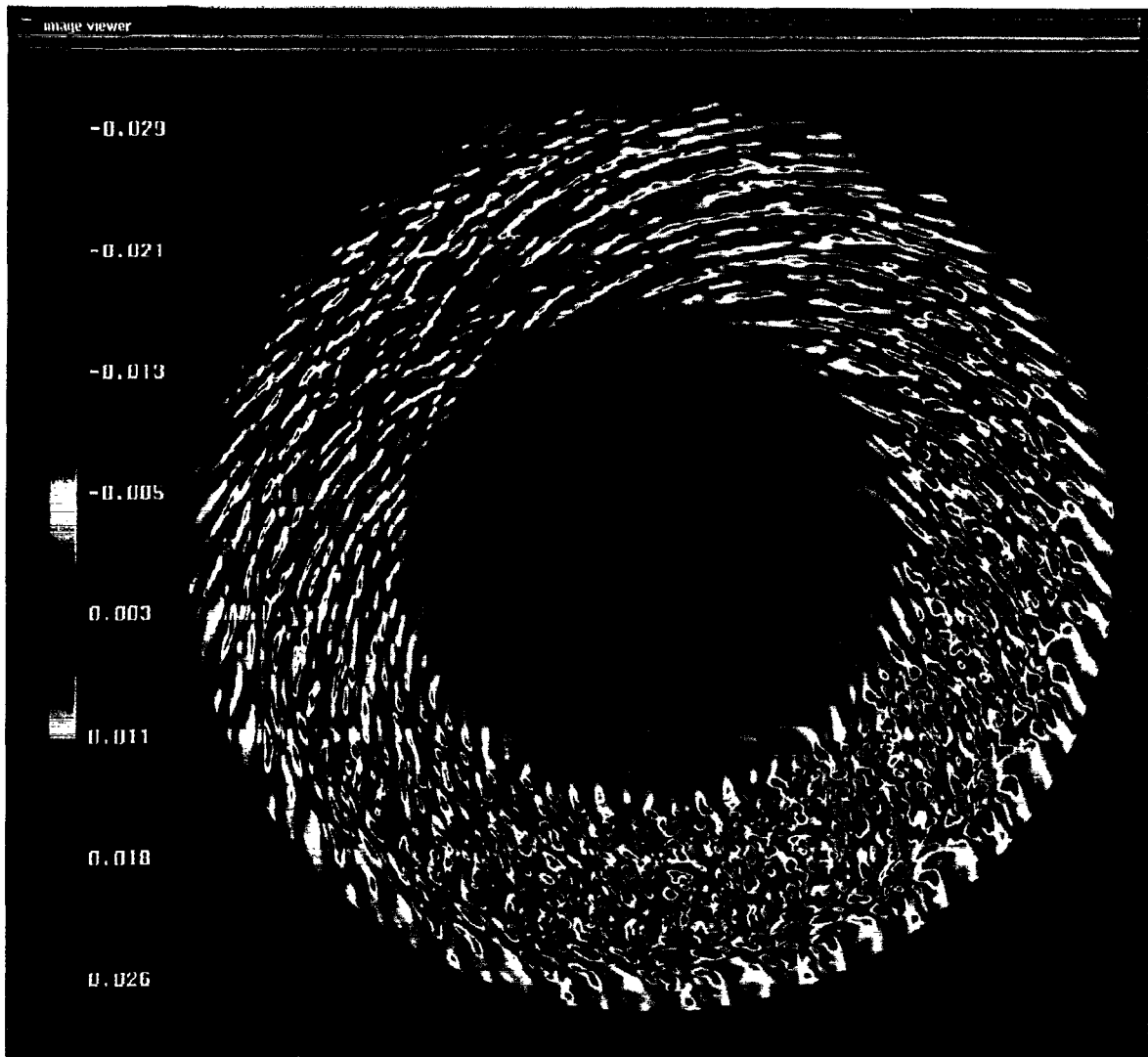
FIG. 8. Instantaneous density contour plots on a constant toroidal angle radial annulus with $\gamma_E = 0.06$ and $\gamma_P = 0$ for the standard case.

the standard case ($q = 1 \rightarrow 4$, $\hat{s} = 2 \rightarrow 0.5$) one variable at a time gives very crudely $D_{ML} \propto (q/\hat{s})^2$. Variations with $2\hat{s} = q$ show D_{ML} nearly constant (see dashed lines). By comparison the slab limit simulations of Ref. 5 can be characterized by $(q/\hat{s})^{1/2}$ at weak shear and $(q/\hat{s})^2$ at strong shear.

Figure 10 shows that the mixing length rule has some credibility near threshold for moderate $q \leq 3$ and strong shear $2\hat{s}^{-1} \leq 2$. Very roughly $\chi \approx 0.5 (q/\hat{s})^2 (c_s \rho_s^2/R)(R/L_T - R/L_{T-crit})$ characterizes the behavior. Specifically we show comparative lines for an adjusted rule $3D_{ML} (D_{ML} = \gamma_{max}/\Delta_x^2)$ and $0.5 (\tilde{p}^a/p_0)_{ML} [(\tilde{p}^a/p_0)_{ML} = \Delta_x/L_P]$. Note that with radial modes included the adjusting coefficients are roughly $O(1)$. If the radial modes were not included, large factors would be needed. However, it is apparent that for high q and particularly for weak shear $2\hat{s}^{-1} \geq 2$, there is considerable saturation and deviation from the mixing length rule. In particular it is clear that there is a smooth approach to finite transport at vanishing shear; $\hat{s} = 0$ is easily accomplished in a BMR code. Periodicity is automatic. The gyroradius cutoff truncates the spectrum in $k_{x'}$. For intermediate and weak shear $k_{x'\ max}$ remains nearly con-

stant. Toroidicity provides localization along the field in θ. Clearly the mixing rule $\Delta_x = 1/(\hat{s} k_y \theta_{RMS})$ makes no sense at vanishing shear. Further it should be apparent that a finite vanishing shear regime implies that the q dependence will not be dependent on the combination $q/\hat{s}$. It is better to think in terms of the total mixing length $\Delta_x = 1/\Delta k_x$ where $\Delta k_x = \Delta k_{x'} + \hat{s} k_y \Delta \theta$ using Eq. (17). There will be a finite spectrum $\Delta k_{x'} = k_{x''RMS}$ giving a finite Δ_x even when $\hat{s}$ vanishes (provided we regard $\Delta \theta$ as bounded). Regions of reverse shear $\hat{s} < 0$ are not uncommon in tokamaks and are generally associated with improved confinement experimentally. This is not surprising since the geodesic curvature term $[\sin(\theta)]$ works against the normal curvature term $[\cos(\theta)]$ for reverse shear [see Eq. (18)] producing less toroidal drive. For the standard case we find considerably less transport for reverse shear: $\chi = 0.31 c_s \rho_s^2/a$ at $\hat{s} = -1.0$ compared to $\chi = 1.9 c_s \rho_s^2/a$ at $\hat{s} = 1.0$ and $\chi = 0.65 c_s \rho_s^2/a$ at $\hat{s} = -0.5$ compared to $\chi = 2.1 c_s \rho_s^2/a$ at $\hat{s} = 0.5$.

Figure 11 shows a substantial deviation from the mixing length rule for very strong temperature gradients making it difficult to characterize the threshold function in the form of
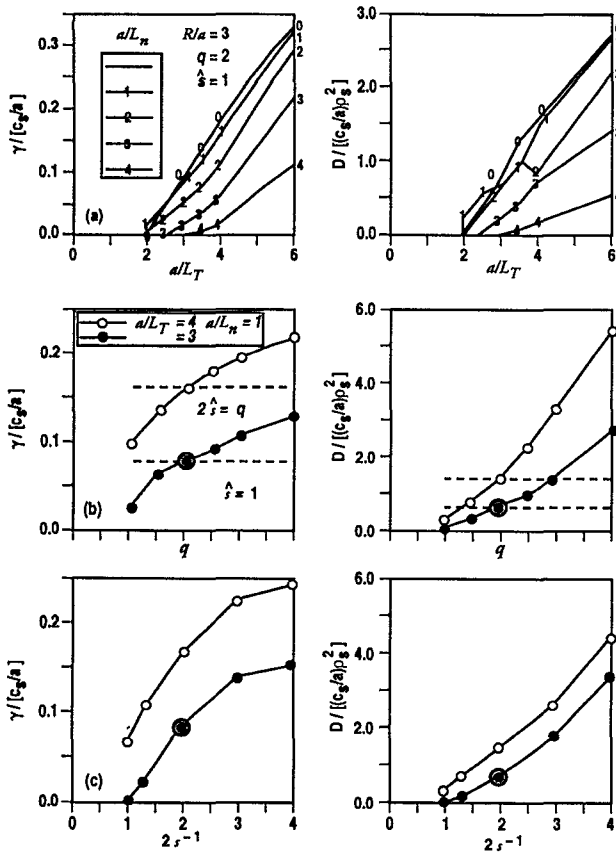
FIG. 9. Parametric dependence of growth rate and mixing model diffusivity. Maximum growth rate and mixing model diffusivity versus temperature gradient (a) versus safety factor q (b); versus inverse shear parameter $(\hat{s})^{-1}$ (c).
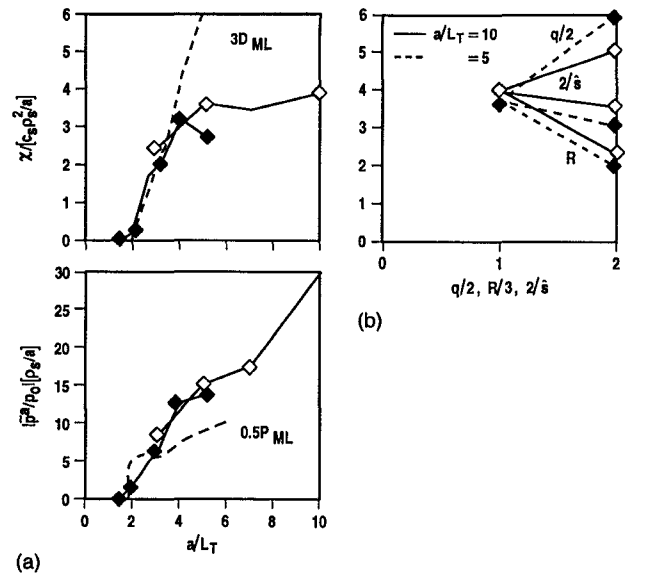

FIG. 11. Simulated points for flux surface diffusivity (top panels) and pressure fluctuations (lower panels) versus a/L_T (a) and versus q, R, and $\hat{s}$ variations (b), standard parameters unless specified.

a power law $(R/L_T - R/L_{T\_crit})^e$. Indeed the exponent appears to go from $e = 1$ to 0 rather abruptly beyond $R/L_T \geqslant 15$. The saturated gradient regime is characterized by a condensation of the spectrum to lower and lower $k_{y'}$ and the $k_{y'}$ grid must be downwardly adjusted. The scaling in the saturated regime appears to be $\chi \approx 6qc_s\rho_s^2/R$ with a very weak dependence on $\hat{s}$. Clear the scaling combination $q/\hat{s}$ is broken. Because of the independence from L_T, $\chi \propto 1/R$ is a
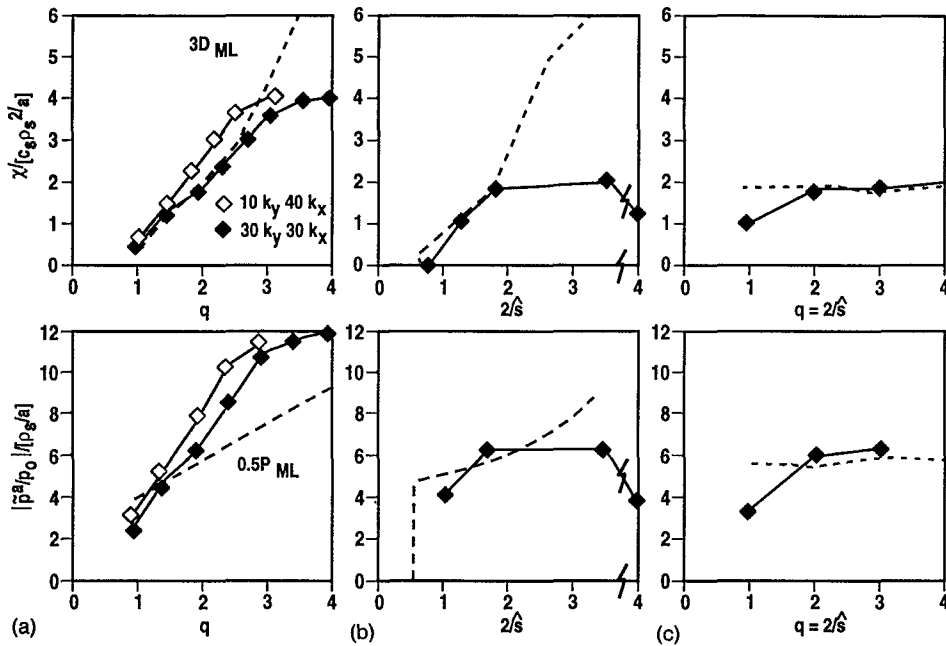

FIG. 10. Simulated points for flux surface diffusivity (top panel) and pressure fluctuations (lower panels) with standard case parameters versus q at $\hat{s} = 1$ (a); versus $2/\hat{s}$ at $q = 2$ (b); versus $q = 2/\hat{s}$ (c). Solid lines without points are $3D_{ML}$ and $0.5\,P_{ML}$. The broken axis points on the middle panels (b) correspond to $2/\hat{s} = 4$ and ∞.

Phys. Plasmas, Vol. 1, No. 7, July 1994

Waltz, Kerbel, and Milovich   2241

TABLE III. TFTR benchmark cases.

	TFTR-1	TFTR-2	TFTR-3
R/a	2.8	3.06	3.06
a/L_n	0.89	1.91	0.278
a/L_T	3.57	4.4	5.83
q	2.4	1.5	1.5
$\hat{s}$	1.5	0.75	0.75
T_i/T_e	1	1.5	0.885
r/a	0.57	0.357	0.357
ρ_s/a	0.001 49	0.0028	0.002 35
a(m)	0.92	0.8	0.8
B(T)	3.8	4.8	4.8
$n(1/\mathrm{m}^{-3})$	3.30E+1.9	3.05E+1.9	4.00E+19
T_e(keV)	1.3	5.7	4.1
Z_{eff}	2.2	3.8	2.7
$\chi_{\mathrm{eff}}^{\mathrm{exp}}/(c_s\rho_s^2/a)$	7.9	1.24	1.53
$\chi_{\mathrm{eff}}^{\mathrm{sim}}/(c_s\rho_s^2/a)$	2.57(1.99)	2.16(1.69)	1.89(1.99)
$\langle \tilde{p}^a/p\rangle/(\rho_s/a)$	8.47(6.94)	9.67(7.67)	10.5(9.5)
$\tilde{n}/n_0(\theta)/(\rho_s/a)$	9.18(7.00)	8.57(7.03)	8.22(7.90)

FIG. 12. Linear growth rate spectrum for TFTR-1 case from gyrokinetic code.

further confirmation of gyro-Bohm scaling as no other length but ρ_s can dimensionally balance R.

Unfortunately it is not at all clear how to merge the saturated regime formula, the threshold regime formula, and account for the saturated behavior at weak shear with a single formula. More work is needed.

D. Discussions of TFTR benchmark cases

Considerable effort has been devoted to three TFTR discharge points corresponding to core radii of an L-mode (TFTR-1), a peaked (TFTR-2), and flat (TFTR-3) density phase of a Super Shot. The L-mode shot (#41309 at 4.4 s from Fig. 1 of Ref. 38) is the focus of a Numerical Tokamak Project code comparison (see Ref. 13) and the latter (#44669 at 4.490 and 4.525 s) have been studied in detail.[39] These are deuterium discharges of average purity, moderately low β and collisionality. Relevant normalized and some raw parameters are given in Table III along with experimental and simulated ion χ_{eff}. Other simulation quantities are also given. As already noted we expect more elaborate GLF models which are in closer agreement to kinetic theory to have somewhat higher diffusion. The simulations results for two grids are given as $30k_y\times30k_x(10k_y\times40k_x)$ at $k_{y_{-}\,\mathrm{max}}=1$ and $\hat{\theta}_{\mathrm{max}}=\pi$. The increase in χ_{eff} with increasing k_y grid density is typical of the standard case (see Table II). The simulated transport is not in gross disagreement with experimental results. The Super Shot cases do not show the expected strong dependence on the η_i parameter (2.3 and 21, respectively), perhaps because both cases are far enough into the flat density regime where the dependence on the density profile is weak. However, the close comparison with the Super Shots is likely fortuitous since there is no clear explanation for the disagreement with the L-mode case which experimentally shows considerably poorer confinement.

These results are given here for use as code comparison benchmarks. It seems unlikely that we should expect better agreement with experiments from the idealized physical models used here. To illustrate this point we show the driving rate sp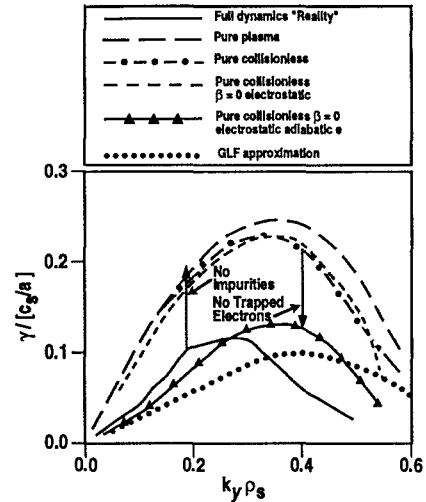ectrum for the L-mode case from Kotschenreuther's gyrokinetic stability code[35] in Fig. 12. This ballooning mode code has the same circular geometry used here, although it is electromagnetic, and retains the effect of trapped particles with pitch angle collisions for electrons, ions, and impurities. It should be easily apparent from the exercise shown, that the potential stabilizing effects of impurities (as well as fast particles) as noted in Ref. 35, are largely offset by the destabilizing effects of the trapped electrons. The β and collisionalities for this particular case are low enough for electrostatic collisionless idealizations, but comparisons with pure ion plasmas having adiabatic electrons seem unwarranted. The near agreement in growth rates between the full physics and our idealizations is simply fortuitous.

VI. SUMMARY

The nonlinear ballooning mode representation BMR seems to offer a clear advantage over previous multiple helicity (m,n,r) representations. Efficient methods for dealing with poloidal periodicity have been demonstrated. We have successfully applied the BMR to a simple gyroaveraged four-moment gyro-Landau fluid model for toroidal ion temperature gradient transport. Extensive case studies have been made around the parameters characteristic of a core tokamak plasma $(a/L_T=3,\ a/L_n=1,\ a/R=1/3,\ T_i/T_e=1,\ q=2$, and $\hat{s}=1)$ in the weak density gradient regime $(R/L_n\geqslant15)$. Keeping in mind the caveats (1) in the use of idealized physics including only a pure ion plasma with adiabatic electrons in the GLF model, and (2) in the use of a BMR which assumes homogeneous turbulence in a narrow radial annulus without convective losses of turbulent energy, several physical conclusions can be drawn:

(1) Inclusion of the nonlinearly generated and linearly damped $n=0$ radial modes (small-scale sheared rotations) causes a tenfold reduction in the transport from finite-n ballooning modes. Magnetic pumping plays no significant role in the radial mode damping. The GLF

Waltz, Kerbel, and Milovich

model with Landau damping for the ballooning modes is applied unchanged to the radial modes. The physics of radial mode generation and damping is crucial and yet to be verified by comparison to gyrokinetic calculations.

(2) Toroidal ITG transport can have twentyfold larger transport than slab ITG transport obtained by dropping the curvature effects. The ballooning effect is very strong with transport flows having a typical 1:10 in–out asymmetry and the turbulence a 1:2 asymmetry.

(3) The simulations are sufficiently independent of the $(k_{x'}, k_{y'})$ grid normalized to the gyroradius that gyro-Bohm scaling with respect to the relative gyroradius ρ_s/a is implied. The BMR simulations effectively operate at vanishing ρ_s/a and do not include the profile effects of inhomogeneous turbulence which in principle could lead to Bohm scaling at finite values of ρ_s/a.

(4) No subcritical turbulence has been found. Close to the temperature gradient threshold for moderate $q \lesssim 3$ and strong shear $\hat{s} \gtrsim 1$ the simulations roughly follow the size and scaling of the mixing length rules $[D_{ML} = \gamma_{max}/\Delta_x^2, (\tilde{p}^a/p_0)_{ML} = \Delta_x/L_P$ with $\Delta_x = 1/(\hat{s}k_y\theta_{RMS})]$. Crudely we can write $\chi \approx 0.5(q/\hat{s})^2(c_s\rho_s^2/R)(R/L_T - R/L_{T\_crit})$

(5) However, for weak shear $\hat{s} \lesssim 1$ there is weak dependence on shear and even vanishing shear has moderate transport. The limit of vanishing shear is easily treated in the BMR formulation. The mixing length rule $\Delta_x = 1/(\hat{s}k_y\theta_{RMS})$ appears to make sense only for strong shear. Reverse shear has considerably less transport as expected from the geodesic curvature working against the normal curvature.

(6) Furthermore there appears to exist a saturated strong gradient regime $R/L_T \gtrsim 15$ with condensation to low k_y and strong deviations from the mixing length rules. Crudely $\chi \approx 6qc_s\rho_s^2/R$ with a weak dependence on R/L_T and $\hat{s}$.

(7) For a core plasma with purely toroidal rotation the parallel flow shear combines with $\mathbf{E} \times \mathbf{B}$ flow shear to give a stabilizing Doppler shear rate $\gamma_E = (r/q)d(V_\phi/R)/dr$ in competition with the Kelvin–Helmholtz parallel shear flow driving rate $\gamma_P \approx dV_\phi/dr$. Doppler shear stabilization can cause ITG transport to vanish if $\gamma_E \gtrsim \gamma_{max}$ including the driving effect of γ_P. This "rule" appears to hold even at vanishing $\hat{s}$.

(8) The poloidal (k_y) and radial (k_x) spectra of outboard density fluctuations appear to be in semiquantitative agreement with BES measurements at core radii of TFTR. The nonvanishing of the low-k_y spectrum (integrated over k_x) is a key signature of the stabilizing radial modes. Asymmetry in the k_x spectrum and a small up-down asymmetry in the outboard turbulence should be an easily identified signature of Doppler shear stabilized transport.

(9) Code benchmark comparison of ion heat diffusivities at core radii from three TFTR discharges shows the simulated transport of comparable size. However, any agreement with TFTR experiments is likely fortuitous since the large stabilizing effects of impurity ions and destabilizing effects of trapped electrons have not been included.

[1] G. W. Hammett and F. W. Perkins, Phys. Rev. Lett. **64**, 3019 (1990).

[2] G. W. Hammett, W. Dorland, and F. W. Perkins, Phys. Fluids B **4**, 2052 (1992).

[3] W. Dorland and G. W. Hammett, Phys. Fluids B **5**, 812 (1993); see also W. Dorland, Ph.D. thesis, Princeton University, 1993.

[4] R. E. Waltz, R. R. Dominguez, and G. W. Hammett, Phys. Fluids B **4**, 3138 (1992).

[5] S. Hamaguchi and W. Horton, Phys. Fluids B **2**, 3040 (1990).

[6] W. Horton, R. D. Estes, and D. Biskamp, Plasma Phys. **22**, 663 (1980); see also W. Horton, D. Choi, and W. Tang, Phys. Fluids **24**, 1085 (1981).

[7] R. E. Waltz, Phys. Fluids **31**, 1962 (1988); see also Phys. Fluids B **2**, 2118 (1990).

[8] S. E. Parker, W. W. Lee, and R. A. Santoro, Phys. Rev. Lett. **71**, 2042 (1993).

[9] S. C. Cowley, R. M. Kulsrud, and R. Sudan, Phys. Fluids B **3**, 2767 (1991).

[10] R. E. Waltz and G. D. Kerbel, in *Proceedings of U.S./Japan Workshop on Ion Temperature Gradient Driven Turbulent Transport*, edited by W. Horton, M. Wakatani, and A. Wootton (American Institute of Physics, New York, 1994), p. 251; see also G. M. Staebler, R. E. Waltz, M. Beer, R. R. Dominguez, W. Dorland, C. M. Greenfield, G. W. Hammett, F. L. Hinton, G. D. Kerbel, T. K. Kurki-Suonio, and J. C. Wiley, in *Plasma Physics and Controlled Nuclear Fusion Research*, Proceedings of 14th International Atomic Energy Agency, Würzburg, 1992 (International Atomic Energy Agency, Vienna, 1993), Vol. 2, p. 329.

[11] M. Beer, G. W. Hammett, W. Dorland, and S. C. Cowley, Bull. Am. Phys. Soc. **37**, 1478 (1992).

[12] G. W. Hammett, M. A. Beer, W. Dorland, S. C. Cowley, and S. A. Smith, Plasma Phys. Controlled Fusion **35**, 973 (1993).

[13] S. E. Parker, W. Dorland, R. A. Santoro, M. A. Beer, Q. P. Liu, W. W. Lee, and G. W. Hammett, Phys. Plasmas **1**, 1461 (1994).

[14] P. H. Diamond and Y. B. Kim, Phys. Fluids B **3**, 1626 (1991).

[15] P. H. Diamond, Y.-M. Liang, B. A. Carreras, and P. W. Terry, "Self-regulating shear flow turbulence: A paradigm for L to H transition," to appear in Phys. Rev. Lett.

[16] B. A. Carreras, V. E. Lynch, and L. Garcia, Phys. Fluids B **3**, 1438 (1991).

[17] P. N. Guzdar, J. F. Drake, D. McCarthy, A. B. Hassam, and C. S. Liu, Phys. Fluids B **5**, 3712 (1993).

[18] A. Hasegawa and M. Wakatani, Phys. Rev. Lett. **59**, 1581 (1987).

[19] W. Dorland, G. W. Hammett, T. S. Hahm, and M. A. Beer, Bull. Am. Phys. Soc. **37**, 1478 (1992); see also W. Dorland, G. W. Hammett, T. S. Hahm, and M. A. Beer in *Proceedings of U.S./Japan Workshop on Ion Temperature Gradient Driven Turbulent Transport*, edited by W. Horton, M. Wakatani, and A. Wootton (American Institute of Physics, New York, 1994), p. 277.

[20] H. Biglari, P. H. Diamond, and P. Terry, Phys. Fluids B **2**, 1 (1990).

[21] K. H. Burrell, E. J. Doyle, P. Gohil, R. J. Groebner, J. Kim, R. J. La Haye, L. L. Lao, R. A. Moyer, T. H. Osborne, W. A. Peebles, C. L. Rettig, T. H. Rhodes, D. M. Thomas Phys. Plasmas **1**, 1536 (1994).

[22] R. J. La Haye, C. L. Rettig, R. J. Groebner, A. W. Hyatt, and J. T. Scoville, Phys. Plasmas **1**, 373 (1994).

Phys. Plasmas, Vol. 1, No. 7, July 1994

Waltz, Kerbel, and Milovich   2243

[23] R. E. Waltz, G. D. Kerbel, G. W. Hammett, and R. R. Dominguez, Bull. Am. Phys. Soc. **36**, 2279 (1991).

[24] S. Hamaguchi and W. Horton, Phys. Fluids B **4**, 319 (1992).

[25] B. Cohen, T. J. Williams, A. M. Dimits, and J. A. Byers, Phys. Fluids B **5**, 2967 (1993).

[26] H. Nordman, V. P. Pavenko, and J. Weiland, Phys. Fluids B **5**, 402 (1993).

[27] R. Linsker, Phys. Fluids **24**, 1485 (1981).

[28] Y. B. Kim, P. H. Diamond, H. Biglari, and J. D. Callen, Phys. Fluids B **3**, 384 (1991).

[29] K. C. Shaing and S. P. Hirshman, Phys. Fluids B **1**, 705 (1989).

[30] J. W. Connor, R. J. Hastie, and J. B. Taylor, Proc. R. Soc. London Ser. A **365**, 1 (1979).

[31] R. Miller and R. E. Waltz, "On the nature of rotational shear stabilization in toroidal geometry and its numerical representation," to appear in Phys. Plasmas.

[32] J. W. Connor, J. B. Taylor, and H. R. Wilson, Phys. Rev. Lett. **70**, 1893 (1993).

[33] G. M. Staebler and R. R. Dominguez, Nucl. Fusion **31**, 1891 (1991).

[34] J. Q. Dong and W. Horton, Phys. Fluids B **5**, 1581 (1993).

[35] M. Kotschenreuther, Bull. Am. Phys. Soc. **37**, 1432 (1991).

[36] J. F. Drake, P. N. Guzdar, and A. Dimits, Phys. Fluids B **3**, 1937 (1991).

[37] R. J. Fonck, Bull. Am. Phys. Soc. **38**, 1960 (1993).

[38] S. D. Scott, V. Arunasalam, C. W. Barnes, M. G. Bell, M. Bitter, R. Boivin, N. L. Bretz, R. Bundy, C. E. Bush, A. Cavallo, T. K. Chu, B. Clinton, S. A. Cohan, P. Colestock, S. L. Davis, D. L. Dimock, H. F. Dylla, P. C. Efthimion, A. B. Errarht, R. J. Fonck, E. Fredrickson, H. P. Furth, R. J. Goldston, G. Greene, B. Grek, L. R. Grisham, G. Hammett, R. J. Hawryluk, H. W. Hendal, K. W. Hill, E. Hinnov, D. J. Hoffman, J. Hosea, R. B. Howell, H. Hsuan, R. A. Hulse, K. P. Jaehnig, A. C. Janos, D. Jassby, F. Jobes, D. W. Johnson, L. C. Johnson, R. Kaita, C. Kieras-Phillips, S. J. Kilpatrick, P. H. LaMarche, B. LeBlanc, R. Little, D. M. Manos, D. K. Mansfield, E. Mazzucato, M. P. McCarthy, D. C. McCune, K. McGuire, D. H. McNeil, D. M. Meade, S. S. Medley, D. Mikkelsen, R. Motley, D. Muller, J. A. Murphy, Y. Nagayama, R. Nazakian, D. K. Owens, H. Park, A. T. Ramsey, M. H. Redi, A. L. Roquemore, P. H. Rutherford, G. Schilling, J. J. Scivell, G. L. Schmidt, J. Stevens, B. C. Stratton, W. Stodiek, E. J. Synakowski, W. M. Tang, G. Taylor, J. R. Timberlake, H. H. Towner, M. Ulrickson, S. von Goeler, R. Weiland, M. Williams, J. R. Wilson, K.-L. Wong, S. Yoshikawa, K. M. Young, M. C. Zarnstorff, and S. J. Zweben, Phys. Fluids B **2**, 1300 (1990).

[39] W. Horton, D. Lindberg, J. Y. Kim, J. Q. Dong, G. W. Hammett, S. D. Scott, M. C. Zarnstorff, and S. Hamaguchi, Phys. Fluids B **4**, 953 (1992).